Dynamic mode decomposition of H-type transition to turbulence

By T. Sayadi, J. W. Nichols, P. J. Schmid† AND M. R. Jovanović‡

For H-type transition to turbulence in a flat-plate boundary layer, we identify dynamically important features resulting from direct numerical and large eddy simulations (DNS and LES, respectively). Even though LES coupled with a dynamic subgrid-scale model provides an accurate prediction of the transition location, it fails to predict initial overshoot and subsequent turbulent skin friction. Dynamic Mode Decomposition (DMD) is used to quantify the contribution of coherent structures to the total Reynolds shear stress. We show that low-frequency modes, corresponding to the legs of hairpin vortices, account for most of the total Reynolds shear stress gradient. We conclude that LES underpredicts the skin friction because the dynamically important low frequency modes do not attain sufficient amplitude.

1. Introduction

Dynamic Mode Decomposition (DMD) is a novel data analysis technique that extracts coherent features from otherwise complicated flows (Schmid 2010). Because DMD is data-driven, it applies to both experimental and numerical data. Given a sequence of flow snapshots, DMD identifies spatial modes which oscillate with a single frequency. In this respect, DMD is somewhat similar to Fourier analysis and shares its broad range of applicability. An important difference, however, is that DMD allows for non-uniformly spaced, complex frequencies, which may involve linear growth and decay. This enables DMD to identify and resolve instabilities and self-sustaining cycles with complex multi-scale behavior.

To further understand the advantages of DMD, it is useful to compare it to another commonly used data analysis technique: Proper Orthogonal Decomposition (POD) (Sirovich 1987; Holmes *et al.* 1996; Moin & Moser 1989). For a sequence of snapshots, POD produces a set of modes such that the residual is minimized with respect to an "energy" norm. Unlike DMD, each POD mode corresponds to a temporal evolution that may contain a range of frequencies. While POD optimally captures the energy of a flow, some flows are strongly affected by temporally coherent, but weakly-energetic, modes. The "natural" (H-type) transition of a flat-plate boundary layer from laminar flow to turbulence is an example of such a flow: weakly-energetic harmonic Tollmien-Schlichting waves undergo secondary instability and then, by extracting energy from the mean shear, grow dramatically before breaking down into turbulence (Herbert 1988).

For engineering applications, it is important to predict the location of the laminar-to-turbulent transition, the level of the skin-friction coefficient through the transition region

† Laboratoire d'Hydrodynamique (LadHyX), École Polytechnique, 91128 Palaiseau cedex, France.
‡ Department of Electrical and Computer Engineering, University of Minnesota, Minneapolis, MN 55455, USA.

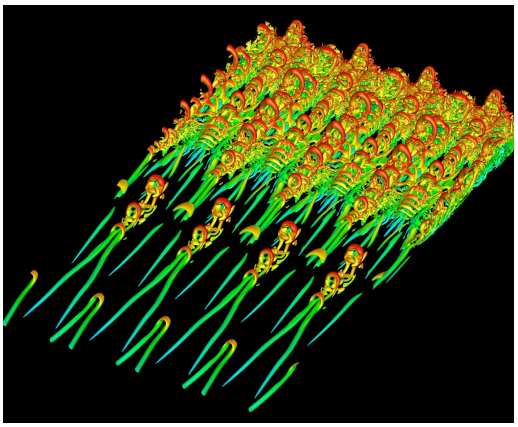

FIGURE 1. Formation of packets of hairpin vortices in H-type transition.

	L_x	L_y	L_z	N_x	N_y	N_z	Δx^+	$\Delta y^+_{\min}$	Δz^+	$Re_{\theta_{\max}}$	λ_z
H-type(DNS)	9.6	1.0	0.605	4096	550	512	10.3	0.41	5.4	1250	0.1514
H-type (LES/UNS)	9.6	0.5	0.1514	480	160	16	90	0.91	42	1250	0.1514

TABLE 1. Characteristics of the different grids.

and the statistical features of the turbulence downstream. Previous work has shown that large-eddy simulation (LES) coupled with a dynamic subgrid-scale (SGS) model provides an adequate prediction of the transition location (Sayadi *et al.* 2011). This represents an improvement over static SGS models, which inhibit transition by introducing unphysically high levels of SGS viscosity in the upstream laminar flow. A remaining difficulty, however, is that the dynamic SGS models tend to underpredict the strength of the transition, and some measures of the turbulence downstream. Visualizations (see Figure 1) of direct numerical simulations (DNS) of H-type boudary layer transition show that Λ-vortices created by secondary instabilities lead to highly organized packets of hairpin vortices in the transition region. Traditional SGS models do not account for this type of coherence, which is considered as the primary reason for the discrepancy between LES and DNS observations.

The purpose of this study is to apply DMD to DNS of natural ("controlled") H-type transition on a zero-pressure-gradient flat-plate boundary layer. In particular, we investigate whether a few dynamically important modes, extracted through DMD, can provide a good estimate of the total Reynolds shear stress. Moreover, applying DMD to LES of the same flow establishes whether these modes are represented correctly with lower resolution; it also provides insight into the effect of SGS modeling on these modes.

2. Methodology

Direct and large eddy simulation of the H-type transition to turbulence is performed using a compressible Navier-Stokes solver for an ideal gas with Sutherland's law for viscosity (Sayadi *et al.* 2011; Nagarajan *et al.* 2003). The inlet Reynolds number based on the distance from the leading edge is $Re_x = 10^5$, and the characteristic length scale used for non-dimensionalization is based on the distance of the inlet station from the

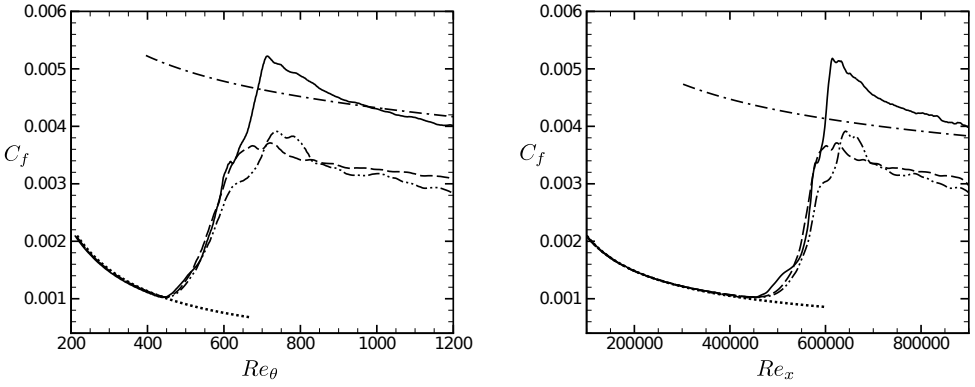

(a) C_f versus Re_θ (b) C_f versus Re_x

FIGURE 2. Streamwise profiles of skin friction: ——, DNS; − − −, LES (dynamic Smagorinsky); − · ·−, UNS; − · −, turbulent correlation $C_f = 0.455/\ln^2(0.06Re_x)$ (White 2006); · · ·, laminar correlation.

leading edge of the plate, $x_0 = 1$. The dimensions of the computational domain are given in Table 1. In order to assess the performance of the dynamic Smagorinsky SGS model, a simulation without any SGS model is performed on the same grid as the LES. This simulation corresponds to an under-resolved numerical simulation with no SGS model, or UNS.

DMD is performed using the algorithm presented in Schmid (2010), with a preprocessing step based on singular value decomposition. This implementation allows for rank-deficient snapshot sequences, and it avoids ill-conditioned companion matrices (Rowley *et al.* 2009). In its simplest form, DMD provides the following representation of a flow field U,

$$U(x, y, z, t) = \sum_{n=1}^{N} a_n \exp(\lambda_n t)\phi_n(x, y, z), \tag{2.1}$$

where $x, y,$ and z are spatial coordinates and t is time. In Eq. (2.1), ϕ_n's are the DMD modes, a_n's are the amplitudes and λ_n's are the frequencies of the respective modes. ϕ_n, a_n, and λ_n are complex-valued quantities.

In DMD, the modes and frequencies are determined without the need for specifying an inner product or a norm. Compared to POD, this gives DMD the advantage of being applicable to any choice of flow quantities or spatial locations. We exploit this fact in section 3.2.

Once the modes and frequencies of the system are computed, we recover the complex amplitudes through a reconstruction of the original data. To solve for the magnitudes of each mode, a_n, we apply a pseudo-inverse to find the bi-orthogonal basis, ψ, of dynamic modes, ϕ such that

$$< \psi_i, \phi_j >= \int \psi_i^* \phi_j dV = \begin{cases} 0, & i \neq j \\ 1, & i = j. \end{cases} \tag{2.2}$$

While this could be done over all snapshots, in this report we choose to apply the pseudo-inverse to the first snapshot only, and then use the remaining snapshots to evaluate the closeness of fit over later times. Multiplying both sides of Eq. (2.1) at $t = 0$ by ψ_n and

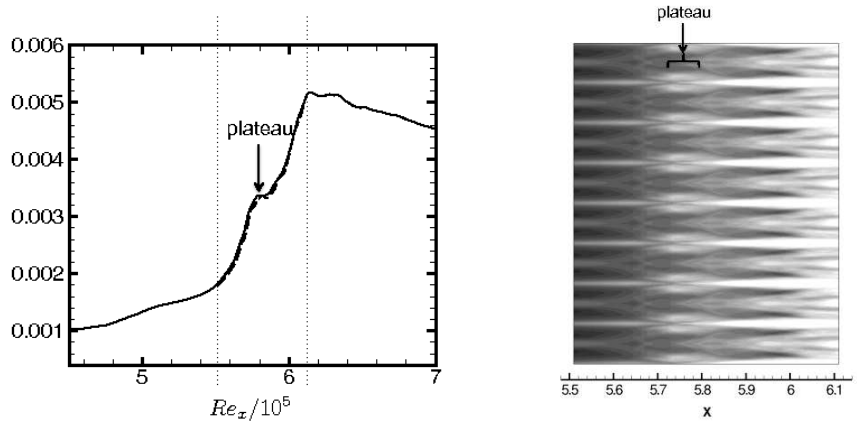

(a) ——, DNS; − − −, first DMD mode (mean). (b) Contours of C_f obtained using the first DMD mode (mean).

FIGURE 3. Skin friction coefficient, C_f (H-type).

using the bi-orthogonal relation (2.2) gives

$$< \psi_n, v_1 >= a_n < \psi_n, \phi_n >= a_n, \qquad n = 1, 2, \cdots, N-1. \tag{2.3}$$

If the dynamic modes are normalized, $|\tilde{a}_n|$ gives the relative magnitude of the n^{th} mode.

3. Results

Figure 2 shows the streamwise development of skin friction from UNS, LES and DNS. Both LES and UNS predict the point of transition accurately. For the early transitional flow, however, the skin friction coefficient predicted by the LES remains in closer agreement with DNS than does the coefficient predicted by UNS. Further downstream, both LES and UNS underpredict the overshoot and turbulent skin friction coefficient.

3.1. *DMD of the skin friction coefficient*

DMD is performed on the two-dimensional skin friction coefficient taken from the DNS data. The streamwise coordinate of the domain used for this analysis extends from $Re_x = 5.5 \times 10^5$ to $Re_x = 6.1 \times 10^5$, between the vertical dotted lines in Figure 3(a). Figure 2(b) shows that this streamwise length coincides with the region where the skin friction starts diverging from the laminar correlation to the location where the skin friction reaches its maximum. Figure 3(a) compares the time- and spanwise-averaged skin friction from the total DNS data (solid curve) to the spanwise-average of the first DMD mode (dashed curve). In the limit of infinitely many snapshots, the first DMD mode is mathematically equivalent to a time-average, so the good agreement shown in Figure 2(a) is expected, and serves as a verification of the method. The spatial structure of the first DMD mode is shown in Figure 3(b).

Figure 4 shows the magnitude of all the DMD modes versus their frequency. This amplitude spectrum identifies four modes (shown in black, together with their complex-conjugates) as dynamically important to the original skin friction signal. The reconstructed skin friction coefficient using these four modes is plotted in Figure 5. The contours of skin friction coefficient from the original DNS data are also plotted in this figure.

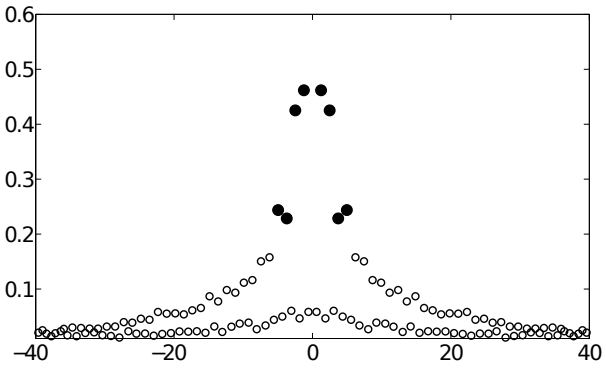

FIGURE 4. Magnitudes, a_n: ○, all modes; •, modes 2,4,6 and 8.

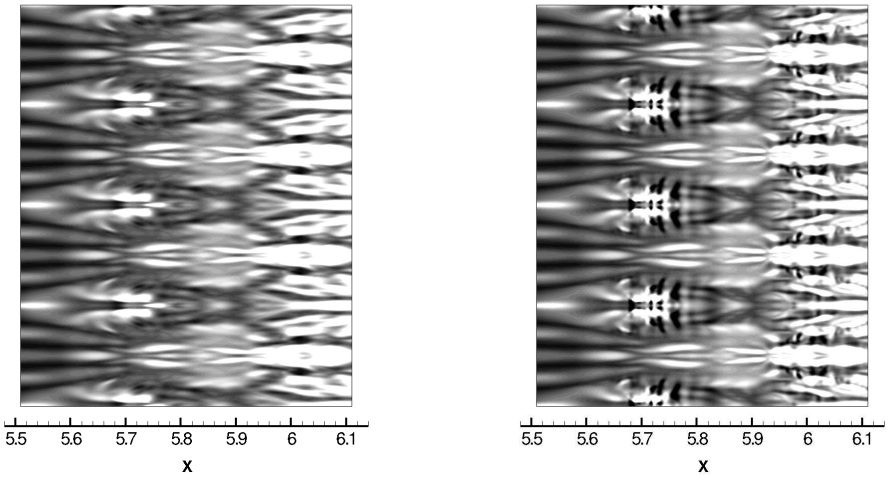

(a) Reconstruction using 8 modes (b) DNS data

FIGURE 5. Contours of instantaneous skin friction.

Comparison of the reconstructed and the original skin friction data shows that four low-frequency modes are able to provide a good approximation of the DNS data.

3.2. *Composite DMD*

In order to identify three-dimensional flow features responsible for the wall skin-friction measured in the previous section, composite DMD is performed on the second invariant of the velocity gradient tensor, Q (Hunt *et al.* 1988), and the skin friction coefficient. DMD rearranges both two-dimensional and three-dimensional fields into column vectors in the snapshot matrix. In the present case, composite DMD means that a vector corresponding to the Q field is simply appended to each of the C_f vectors before performing DMD. As previously mentioned, concatenation of vectors containing quantities of different units is possible because DMD does not require an inner product.

Figure 6(b,e) shows the first three low frequency modes resulting from the composite

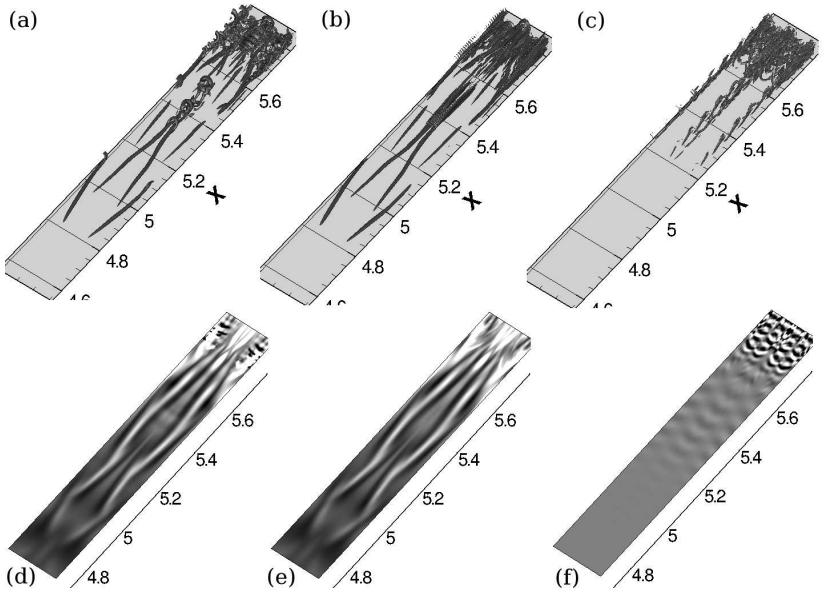

FIGURE 6. Composite DMD: an isosurface of the Q-criterion is shown in the top row and contours of the skin friction coefficient are shown in the bottom row. (a,d): full DNS data; (b,e): superposition of three low-frequency DMD modes; (c,f): a single high-frequency mode.

DMD. Although some small-scale features are missing in the reconstruction, the overall quality of approximation is satisfactory. This figure also shows the structures, through the Q-criterion, of the superposition of these three low frequency modes. While the legs of the hairpin vortices are represented by these low frequency modes, the heads are not represented accurately if at all.

In contrast to the low-frequency modes, Figure 6(f) shows the signature of the skin friction profile from one high frequency mode and its respective structure in the boundary layer. The skin friction profile from this single high frequency mode does not contribute much to the overall skin friction profile. The contours of the skin friction profile of the high frequency modes are an order of magnitude smaller than the original DNS data. The Q-criterion shows that this mode corresponds to the heads of the hairpin vortices in Figure 6(c). This wall normal distribution of frequencies into different layers may be explained by considering the wall-normal dependence of the convection velocity inside the boundary layer. The formation of high frequencies away from the wall that later spread towards the wall is consistent with the mechanism discussed by Bake *et al.* (2002).

3.3. *Triple decomposition*

Triple decomposition originally introduced by Reynolds & Hussain (1972), can be used to decompose a signal into three components,

$$f = \overline{f} + \tilde{f} + f'. \tag{3.1}$$

Here, $\overline{f}$ is the time-averaged component, $\tilde{f}$ is the time periodic component and f' is the component arising from turbulent motion. $\tilde{f}$ is obtained by phase-averaging the data with a specific frequency (resulting in $\langle f \rangle$) such that $\tilde{f} = \langle f \rangle - \overline{f}$. Time- and phase-averaging

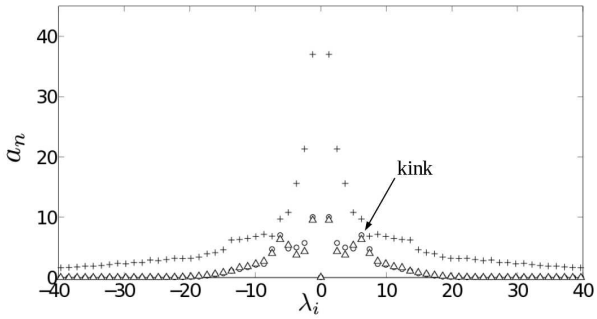

FIGURE 7. Magnitudes: ∘, LES; Δ, UNS; +, DNS.

of the incompressible Navier-Stokes equations yields:

$$\frac{\partial \overline{u}_i}{\partial x_i} = \frac{\partial \tilde{u}_i}{\partial x_i} = \frac{\partial u'_i}{\partial x_i}, \tag{3.2}$$

$$\overline{u}_j \frac{\partial \overline{u}_i}{\partial x_j} = -\frac{\partial \overline{p}}{\partial x_i} + \frac{1}{Re}\frac{\partial^2 \overline{u}_i}{\partial x_j \partial x_j} - \frac{\partial}{\partial x_j}(\overline{u'_i u'_j}) - \frac{\partial}{\partial x_j}(\overline{\tilde{u}_i \tilde{u}_j}). \tag{3.3}$$

Performing a conventional time-averaging operation on the momentum equation would yield the same left-hand side and the first two terms on the right-hand side of Eq. (3.3). The third and fourth terms are combined into the Reynolds shear stress gradient

$$\frac{\partial}{\partial x_j}(\overline{u_i'^t u_j'^t}) = \frac{\partial}{\partial x_j}(\overline{u'_i u'_j}) + \frac{\partial}{\partial x_j}(\overline{\tilde{u}_i \tilde{u}_j}), \tag{3.4}$$

where u'^t is defined as $u'^t = u - \overline{u}$, $\frac{\partial}{\partial x_j}(\overline{u'_i u'_j})$ is the contribution of the turbulent motion and $\frac{\partial}{\partial x_j}(\overline{\tilde{u}_i \tilde{u}_j})$ is the contribution of the coherent motion to the Reynolds shear stress.

In DMD, each mode is sampled based on its specific frequency. We argue that each DMD mode is an optimal phase-average at its respective frequency. Based on this description, the contribution of each DMD mode to the Reynolds shear stress is the coherent motion from one specific phase-average. The contribution of the n^{th} coherent structure to the total Reynolds shear stress is evaluated by $\frac{\partial}{\partial x_j}(\overline{\tilde{u}_i^n \tilde{u}_j^n})$, where n represents the n^{th} DMD mode. Our aim is to assess whether a reduced order model consisting of a few DMD modes ($n << N$) can reliably capture the Reynolds shear stress and skin friction profiles.

DMD in the context of triple decomposition is applied to the velocity components of the DNS data of H-type transition as well as LES and UNS of the same flow configuration. The magnitude spectrum of the DMD is shown for these three data-sets in Figure 7. This figure shows that the magnitudes of the modes are underpredicted in LES and UNS. However, the frequencies seem to be correctly captured by both LES and UNS.

In Figure 6, we observed that the superposition of three low-frequency DMD modes provided a good estimate of the the skin friction. Here, we choose the same three low-frequency modes to construct the Reynolds shear stress at $x = 5.68 \times 10^5$. Figure 8 shows that these modes from are also sufficient to approximate the total Reynolds shear stress gradient. The first three DMD modes from LES and UNS, on the other hand, dramatically underpredict the total Reynolds shear stress. Although, LES seems to give a better estimate of this value than UNS. The shape of the Reynolds stress profile from LES is similar to the DNS profile, however, to within a multiplicative factor. This indicates

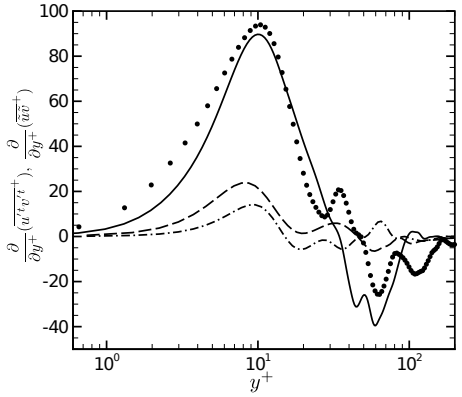

FIGURE 8. Reynolds shear stress gradient: •, DNS; and three low-freqency DMD modes from ——, DNS; − − −, LES; − · −, UNS.

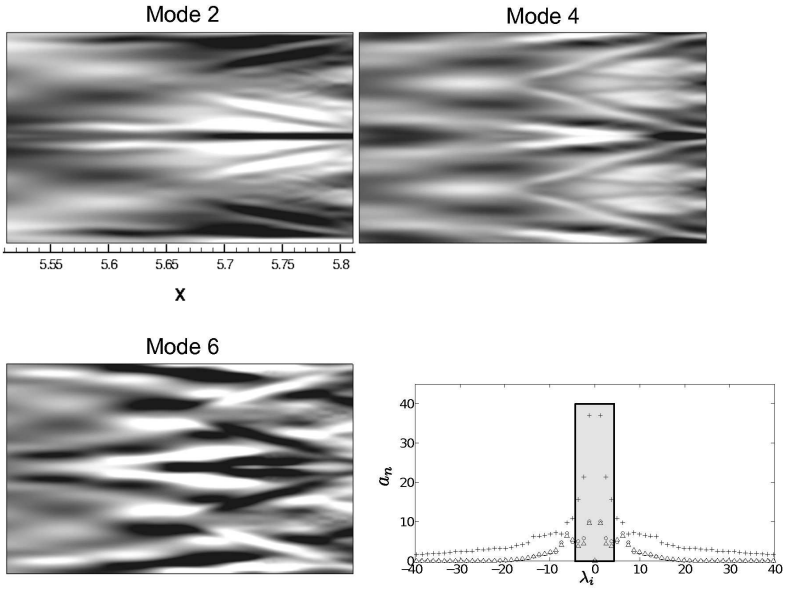

FIGURE 9. Contours of wall-normal velocity

that the underprediction of the skin friction owes only to an underprediction of the magnitudes of each DMD mode. The shape of the three modes extracted from the DNS are shown in Figure 9 using contours of wall-normal velocity. These low frequency modes correspond to large scale structures in the flow.

To investigate whether or not the underprediction of the Reynolds shear stress owes to the underpredicted magnitude instead of the modal shape itself, each of the three low-frequency modes are multiplied by the ratio of the DNS value to that of the first low-frequency mode. Figure 10(a) shows that while rescaled LES modes do a reasonable

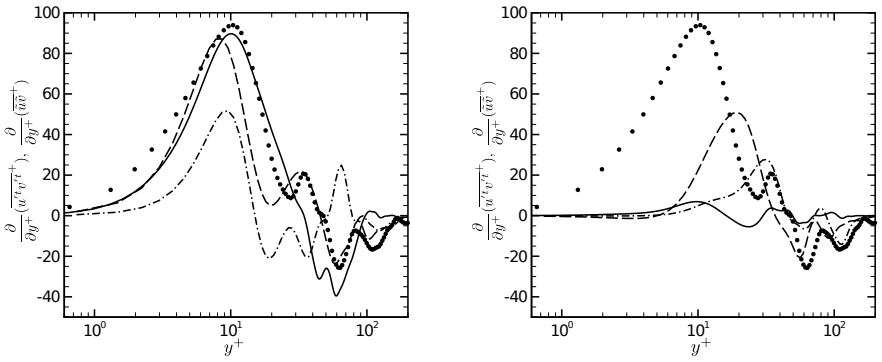

(a) Rescaled Low frequency modes (b) High frequency mode

FIGURE 10. Reynolds shear stress gradient: •, DNS; ——, DMD modes from DNS; − − −, DMD modes from LES; − · −, DMD modes from UNS.

job in approximating the total Reynolds shear stress profile, the performance of UNS is less satisfactory. In particular, the Reynolds shear stress profile remains underpredicted. The fact that the LES modes recover the shape of the DNS wall-normal Reynolds stress profile to within a scaling factor is encouraging from a modeling perspective.

Figure 7 shows a kink in the spectrum of the LES and UNS which is not apparent in the DNS spectrum. The contribution to the total Reynolds shear stress from this relatively high frequency mode is shown in Figure 10. At this frequency, the DNS mode has a very small contribution to the total Reynolds shear stress value. The mode from UNS has a higher contribution but the LES mode has the highest contribution of all. This suggests that the LES model artificially magnifies higher frequency modes at the expense of dynamically important lower frequency modes.

To determine the generality of these results, a future work will perform the same exercise on the DNS data of K-type transition (Sayadi *et al.* 2011). In addition to the dynamic Smagorinsky model, several widely used dynamic SGS models have also been investigated by Sayadi & Moin (2011) in the context of H-type transition, and may be used to assess the effect of different SGS models on the shapes and frequencies of the LES modes. If these results prove to be general across different transition scenarios and SGS models, these low frequency modes can be used as an alternative wall model in the vicinity of the transition region, providing the correct amount of Reynolds shear stress.

4. Conclusions

DMD is performed on the two-dimensional skin friction data of the DNS of H-type transition to turbulence. With few low frequency modes the skin friction profile is estimated accurately. DMD on the composite Q and skin friction data shows that these low frequency modes are associated with the legs of hairpin vortices inside the boundary layer. High frequency modes do not affect the total skin friction coefficient significantly and represent the heads of the hairpin structures. DMD, interpreted in the context of triple decomposition (Reynolds & Hussain 1972), is performed on the velocity components of the DNS, LES and UNS data. The total Reynolds shear stress is approximated correctly by three low frequency modes in the case of the DNS data. The same low frequency modes in LES and UNS underpredict the value of the Reynolds shear stress

gradient. The spectrum of LES and UNS shows a kink at a relatively high frequency. While this relatively higher frequency mode has no contribution to the total Reynolds shear stress in the DNS data, it is artificially magnified through the use of the dynamic Smagorinsky SGS model.

Acknowledgments

The authors acknowledge the computing time provided by the Certainty cluster at Stanford University, funded under the American Recovery and Reinvestment Act of 2009.

REFERENCES

Bake, S., Meyer, D. G. W. & Rist, U. 2002 Turbulence mechanism in Klebanoff transition: a quantitative comparison of experiment and direct numerical simulation. *J. Fluid Mech.* **459**, 217–243.

Herbert, T. 1988 Secondary instability of boundary layers. *Ann. Rev. Fluid Mech.* **20**, 487–526.

Holmes, P., Lumley, J. L. & Berkooz, G. 1996 Turbulence, coherent structures, dynamical systems and symmetry. In *Cambridge Monographs on Mechanics*. Cambridge Univ. Press.

Hunt, J. C. R., Wray, A. A. & Moin, P. 1988 Eddies, stream, and convergence zones in turbulent flows. *Center for Turbulence Research Report CTR-S88* pp. 193–208.

Moin, P. & Moser, R. D. 1989 Characteristic-eddy decomposition of turbulence in a channel. *J Fluid Mech.* **200**, 471–509.

Nagarajan, S., Lele, S. K. & Ferziger, J. H. 2003 A robust high-order compact method for large eddy simulation. *J Comp. Phys.* **191** (2), 392–419.

Reynolds, W. C. & Hussain, A. K. M. F. 1972 The mechanics of an organized wave in turbulent shear flow. part 3. theoretical models and comparisons with experiments. *J Fluid Mech.* **54** (02), 263–288.

Rowley, C. W., Mezic, I., Bagheri, S., Schlatter, P. & Henningson, D. S. 2009 Spectral analysis of nonlinear flows. *J Fluid Mech.* **641**, 115–127.

Sayadi, T., Hamman, C. W. & Moin, P. 2011 Direct numerical simulation of K-type and H-type transitions to turbulence. *Center for Turbulence Research Annual Research Briefs* .

Sayadi, T. & Moin, P. 2011 Predicting natural transition using large eddy simulation. *Center for Turbulence Research, Annual Research Briefs* .

Schmid, P. J. 2010 Dynamic mode decomposition of numerical and experimental data. *J. Fluid Mech.* pp. 1–24.

Sirovich, L. 1987 Turbulence and the dynamics of coherent structures. *Q. Appl. Math.* **45**, 561–590.

White, F. M. 2006 Viscous fluid flow. McGraw-hill International Edition, Third Edition.